JOURNAL OF GEOPHYSICAL RESEARCH, VOL. 115, D14126, doi:10.1029/2009JD013741, 2010

South Pole paleowind from automated synthesis of ice core records

R. C. Bay,[1] R. A. Rohde,[1] P. B. Price,[1] and N. E. Bramall[2]

Received 21 December 2009; revised 18 February 2010; accepted 16 March 2010; published 31 July 2010.

[1] We develop a fully automated reconstruction of South Pole surface roughness as a measure of past wind intensity, using dynamic warping feature recognition and internal consistency checks to reduce subjectivity and analysis time. We synchronized millimeter-resolution optical profiles of deep South Pole glacial dust together with ice core data between the ages 26 and 90 thousand years B.P. The images were captured using a laser dust logger in six boreholes of the IceCube neutrino detector array, a massive construction project in the ice at South Pole and an unusual opportunity for glaciology and paleoclimate research. South Pole surface roughness anticorrelated with curves of Antarctic pCO_2 and temperature, which we propose were connected through secular migrations of the Southern Hemisphere westerlies. This new paleoclimate signal may be direct evidence of atmospheric reorganization during the glacial, helping to deconvolve the thermodynamics and biogeochemistry of climate change. We also found that local intensity of atmospheric circulation roughly tracked the quantity of wind-borne particulates deposited in Antarctic ice during the glacial period, although the largest dust increases were likely furnished by the source regions.

Citation: Bay, R. C., R. A. Rohde, P. B. Price, and N. E. Bramall (2010), South Pole paleowind from automated synthesis of ice core records, *J. Geophys. Res.*, *115*, D14126, doi:10.1029/2009JD013741.

1. Introduction

[2] Wind is a critical environmental parameter and driver of climate, apportioning heat and moisture throughout the atmosphere and ocean, disturbing ocean stratification and influencing pCO_2 exchange. The atmosphere transports roughly half of the poleward heat flux. Dust particles in the atmosphere directly alter the planetary radiation balance, but also indirectly affect climate by delivering nutrients over remote ocean surfaces to influence primary production. Atmospheric dust concentration, as preserved in Antarctic and Greenlandic ice, was one to two orders of magnitude higher during glacial periods than present levels, which has sparked continuing debate over the exact causes [e.g., *Marino et al.*, 2008; *Fischer et al.*, 2007b; *Petit et al.*, 1999]. Local environmental changes at the dust source regions, such as increased aridity and lower sea level, are often invoked as the explanation. However, since dust is carried by wind, more vigorous circulation during colder glacial climates is also likely to have enhanced atmospheric dust content.

[3] Redistribution of snow by the wind impacts glacier mass balance and sweeps polar precipitation into the sea [*Giovinetto et al.*, 1992]. At any site chosen for drilling an ice core, wind in the past will have sculpted snow surface drifts (sastrugi) and degraded continuity of the preserved climate record. Traces of explosive events like volcanic fallout layers may have been removed entirely from a particular core sample. Pressure gradients in the firn created by "wind pumping" drive convection and affect the gas-age ice-age discrepancy, a critical quantity for determining the phase of abrupt climate changes observed in ice [*Brook et al.*, 2005; *Kawamura et al.*, 2006].

[4] Direct proxies of paleowind intensity are lacking and knowledge of past atmospheric circulation is mostly inferred. *Barnes et al.* [2006] described a method for reconstructing past wind speed at Dome C, where serendipitously, two side-by-side ice cores were retrieved after the first drill became stuck. By matching features between two or more nearby core records at high temporal (depth) resolution, the standard deviation of isochrone depth provides a measure of surface roughness as a record of paleowind intensity. Here we analyze fine-structure deviations between ten high-resolution South Pole dust profiles from six boreholes 200 to 950 meters apart and covering the period 26,000 to 90,000 years B.P. We imaged dust scattering and absorption using a laser optical borehole dust logger [*Bramall et al.*, 2005], during construction of the IceCube km^3 neutrino detector array between December 2005 and January 2009.

[5] The IceCube neutrino observatory is the largest particle detector in the world, ~0.7 km^3 as of January 2009. IceCube uses a 5 MW hot-water drill to embed optical sensors between 1450 and 2450 m depth at South Pole, for the purpose of tracking high energy charged particles which traverse the ultra-clean ice. To maximize performance of the telescope, as IceCube expands we are mapping the ice optical variations in detail [*Ackermann et al.*, 2006; *Bramall et al.*, 2005]. With 59 deep boreholes drilled to date and another 21 planned, encompassing an effective volume ~2.5 km^3, IceCube pre-

[1]Department of Physics, University of California, Berkeley, California, USA.
[2]NASA Ames Research Center, Moffett Field, California, USA.

0148-0227/10/2009JD013741

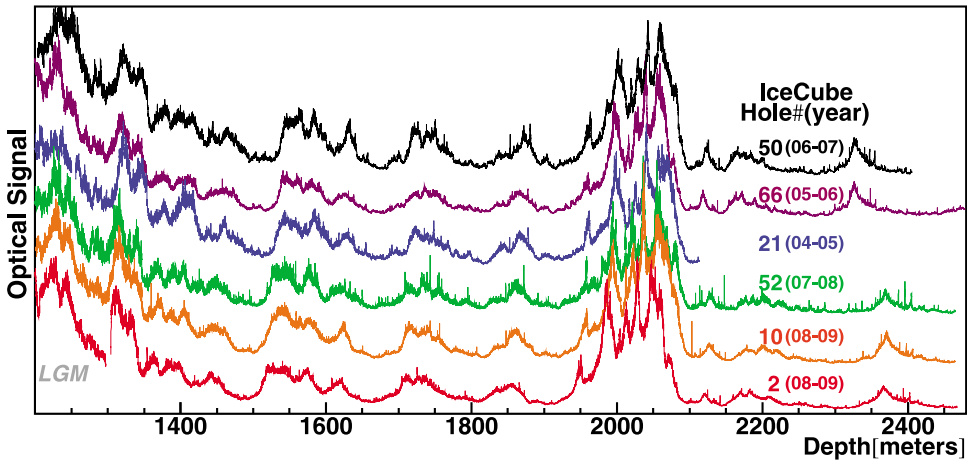

Figure 1. Six of ten deep borehole optical profiles of South Pole dust taken since 2004. Early stages of the Last Glacial Maximum are on the left side. Numerous sub-centimeter features have been resolved in repeated measurements.

sents a unique opportunity for a multi-borehole study of deep glacial ice. On almost all deep ice coring missions, only a single core is retrieved from each drilling site.

[6] Replicate ice core measurements which are separated by lateral distance, whether millimeters away in the same core or thousands of kilometers away at another geographic location, are climatically and glacially related but distorted with respect to one another by variations in both signal amplitude and timing. Classical treatments can be used to deal with amplitude discrepancies, but ice core data are most often synchronized by inspection. Although the human brain, as a highly interconnected parallel processor, is remarkably effective at synthesizing imperfect patterns in small tasks [*Winkler et al.*, 2008; *Kogan and Margoliash*, 1998], manual interpretation of our dust records, comprising millions of data points, would be far too time consuming and susceptible to bias. We develop a fully automated technique for the alignment of a large ice core data set, to derive a first comprehensive record of glacial South Pole surface roughness and wind intensity.

2. Data

[7] A new borehole optical dust logger described by *Bramall et al.* [2005] uses a computer-controlled 404-nm laser line generator, digital photon counter for light detection and precision pressure sensor for depth determination. Annular black nylon brushes function as baffles to intercept stray photons and sweep detritus, particularly ice crystals, from the light path. We made ten optical dust profiles in IceCube boreholes 21, 50, 66, 52, 10 and 2 between 2004 and 2009 (Figure 1). Figure 2 shows the surface locations of the six logged boreholes across the IceCube array. To log Holes 21 and 50 we permanently affixed the probe to a detector string and acquired data while the string was lowered into the ice; during the first log, in Hole 21, telemetry with the probe was lost below 2113 meters. In the four subsequent boreholes we used a separate logging winch to deploy a ruggedized instrument which we could hoist back to the surface, making profiles on both the down and up trips and recovering the device. Data were sent as 10-ms samples (~100 Hz) to a laptop computer at the surface using DSL communication. Logging depth was reconstructed from both pressure readings and winch payout, surveys of the snow surface, well distance to the top of the water column and corrections for water compressibility and cable stretch. Although absolute depth accuracy was limited to a meter or so, the relative uncertainty over moderate depth intervals was negligible.

[8] The dust logger makes a high definition time series image of the optical effects due to particulates and bubbles in ice integrated over an area of order m^2 of the horizon. Our method reveals fine-scale climate variations, trace fallout layers, and subtle trend changes which may be missed in ~0.01 m^2 cross-sections of a single ice core sample. The optical dust profiles we obtained at South Pole are highly repeatable and correspond closely with dust measurements in EPICA ice cores taken at Dronning Maud Land (EDML) and Dome C (EDC) [*EPICA community members*, 2004, 2006]. The laser is spread into a fan shape over ~60° of the horizon, so different passes of the probe may interrogate different ice. Residual air bubbles reduce the contrast of dust scattering and make unambiguous identification of dust horizons increasingly difficult shallower than about 1200 m and into the Last Glacial Maximum around ~1150 m. In the top 1200 meters the optical signal is most useful as an indicator of absorptive anomalies, particularly thin opaque layers from explosive fallout events like volcanic eruptions. For this analysis we exploited a clear fallout layer signal in the bubble-clathrate transition region ~1210 m as a tie point, one which we identified as an interesting horizon climatologically around 26,500 years B.P. [*Bay et al.*, 2006].

[9] We found dust layer tilting across the array along a NE-SW direction of as much as 70 m per lateral kilometer (Figure 3), consistent with stratigraphic undulations detected by aerial radar profiling [*Bingham et al.*, 2007]. Although the South Pole is categorized as a glacial tributary with surface velocity 10.1 m per year, the site lies in a basin surrounded by glacial source region ices with flow velocities $\ll$10 m per year, [*Bingham et al.*, 2007]. We assume that the deeper ice originated in the same general vicinity as the shallower ice and that the entire record can be treated a coherent whole.

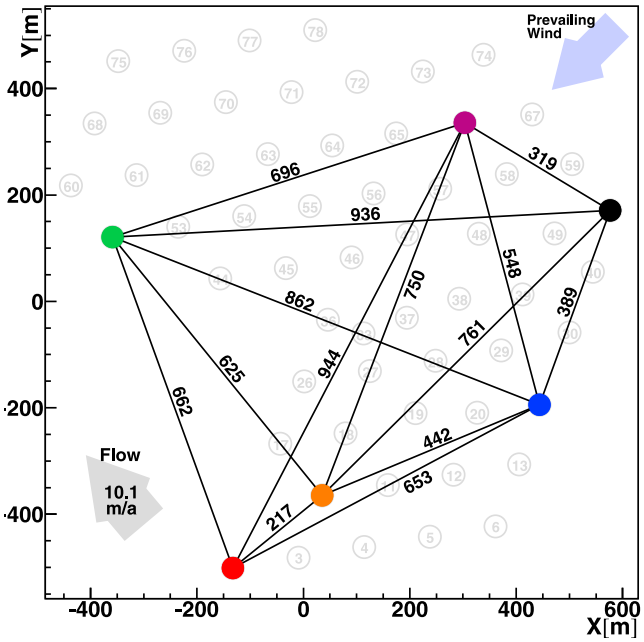

Figure 2. Aerial view of surface locations of each IceCube string deployed as of January 2009. Solid circles color-coded with Figure 1 indicate the boreholes logged, with interhole distances specified for most pairwise combinations. The y-axis is "Grid North" and points to Greenwich, UK; the origin of the IceCube coordinate system was 494 m north and 970 m west of the South Pole (1089 m along 63°W longitude) on January 1, 2009. Surface ice flow velocity is 10.1 m a^{-1} along 310° (approximately NW). Prevailing wind is NE.

South Pole firn is unusually thick (>100 m) [*van den Broeke*, 2008], because of a combination of low mean annual temperature (−48°C at the modern surface) and relatively high accumulation rate. Present South Pole accumulation is approximately log-normal with annual mean 7–8 cm of water equivalent, about 20–25 cm of snow [*Hogan and Gow*, 1997; *van der Veen et al.*, 1999]. The prevailing wind is NE with little variation in direction [*Mahesh et al.*, 2003].

3. Automated Surface Roughness Analysis

3.1. Dynamic Warping Feature Recognition

[10] Dynamic time warping (DTW) presents an appealing solution for synchronization of ice core records, which are presumed to be stratigraphically contiguous (time sequential) but are not in fact continuous. DTW has commonly been applied to biometrics such as speech, gait or handwriting, as a means of overcoming small dynamic variations in order to discover characteristic traits. In voice recognition for example, DTW can be useful when authenticating a speaker against a template voiceprint, notwithstanding fluctuations in tempo, cadence or absolute pitch. Dynamic warping algorithms search for the most efficient mapping between each point in one time series to a point or points in the other, that aligns the trajectories to minimize Euclidean distance and extracts the deformation in a virtually nonparametric way. With iterative deepening [*Keogh and Pazzani*, 2000; *Salvador and Chan*, 2004], two time series can be analyzed at progressively finer resolution over shorter subintervals by feeding back mappings from previous iterations for input seeds. Computational complexity increases only as the square of the number of data points, so that the *entire* 2D warping space can be explored effectively with a fast PC to discover an optimal path.

[11] The optimum warping path w minimizes the cumulative *match distance*, expressed as a cost function $C(w)$, between time series r_i and t_j:

$$C(w) = (1-\alpha)^2 [r_i - t_j]^2 + \alpha^2 \left[\frac{r_i'}{||r_i'||_\infty} - \frac{t_j'}{||t_j'||_\infty} \right]^2 + \beta P(w) \quad (1)$$

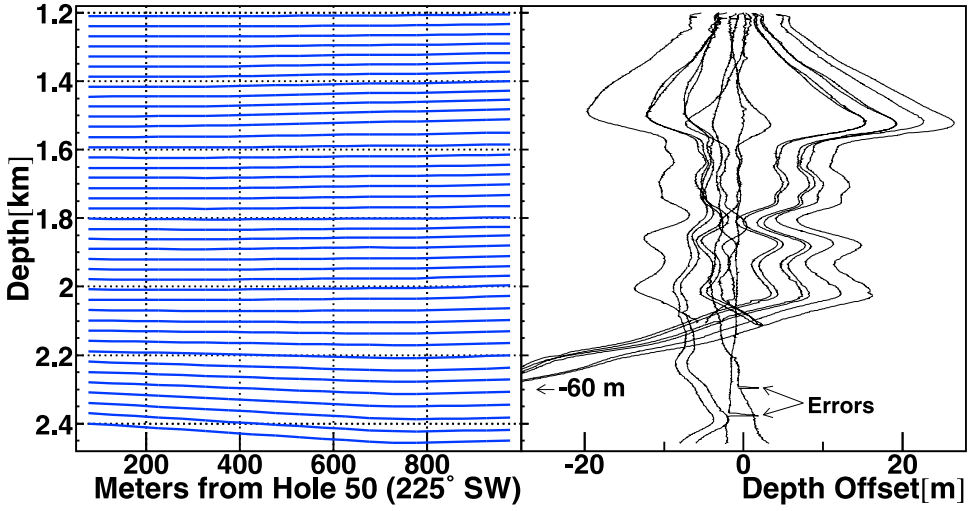

Figure 3. (left) Stratigraphic distortions across IceCube, of as much as 70 meters per lateral kilometer, lie mainly along a NE-SW direction. (right) Condensed subset of interlog maps rendered by the warping algorithm. Offsets are largely the results of ice flow or megadunes and substantial departures from these smooth distortions are typically errors. Wind related surface features are barely perceptible at the scale of the plot.

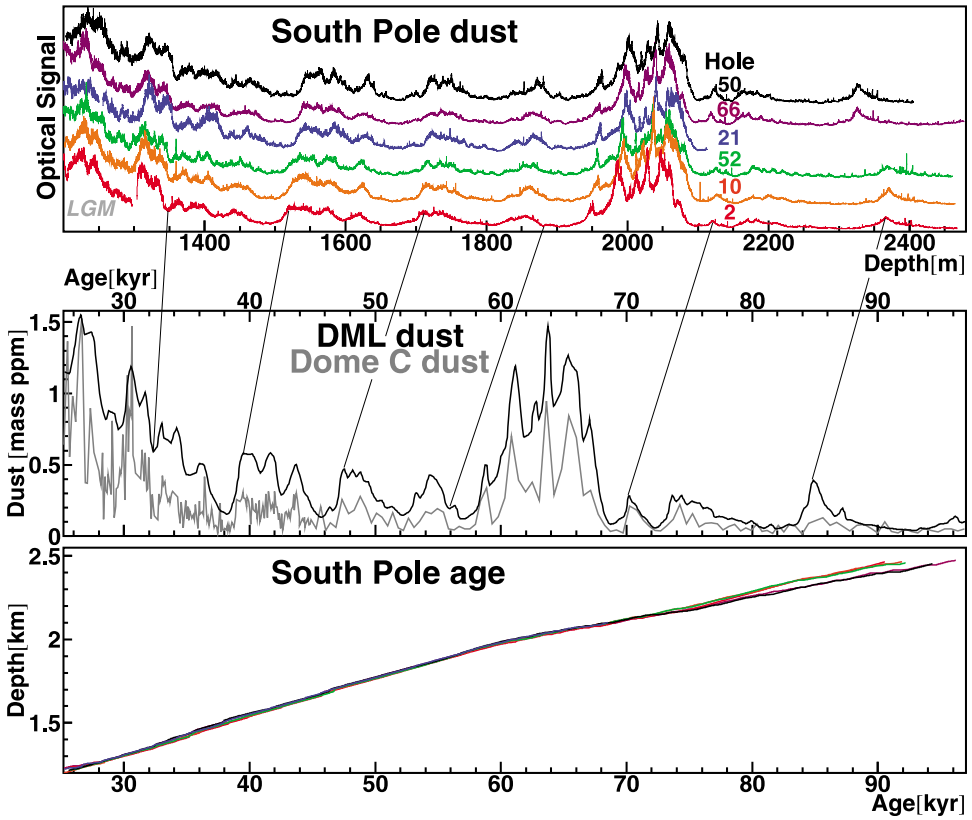

Figure 4. (top) Dating of the South Pole optical profiles, using DTW synchronization to (middle) dust measured in the EDML and EDC ice cores, reaches (bottom) nearly 100 kyr before present. A few tie lines are drawn between dust profiles to guide the eye. The South Pole glacier is >2800 m thick and likely contains ice from the Eemian, a period 130 to 114 ka analogous to the present Holocene.

with parameters $0 \le \alpha \le 1$, $0 \le \beta \le 1$, supremum norm $\|r_i'\|_\infty \equiv \max(|r_i'|)$ and warping penalty $P(w)$ defined by:

$$P = \begin{cases} 1 & r_i,\ r_{i+1} \mapsto t_j \quad \text{or} \quad t_j,\ t_{j+1} \mapsto r_i \\ 0 & r_i \mapsto t_j,\ r_{i+1} \mapsto t_{j+1}, .. \end{cases} \tag{2}$$

That is, we exact a penalty β for mapping two consecutive points in one time series to the same point in the other time series. The two series r_i and t_j are normalized to their arithmetic means and preprocessed to ensure derivatives r_i' and t_j' are well-behaved. Our cost function resembles others developed previously [*Roberts et al.*, 1987; *Witkin et al.*, 1987; *Wang and Gasser*, 1997]. We integrated our cost function with Matlab interpolation DTW shareware (P. Mico, Matlab central file exchange, 2008, http://www.mathworks.com/matlabcentral/fileexchange/16350-continuous-dynamic-time-warping), adding the second and third terms of equation (1). To reduce processing time, we constrained exploration of warping space to reject excessively warped paths, after *Sakoe and Chiba* [1978].

[12] Beginning with the optical dust records dissolved by a factor 2^9 (512 point averaging), we continually refined the optimum warping path with sixteen iterations culminating at full (~2 mm effective) resolution. We found that the parameter α, which adjusts the relative weight placed on the primary signals versus first derivatives, worked best in the range 0.5 to 0.9. To cope with fluctuating normalization of the optical profiles, we strongly emphasized the first derivative (α = 0.9) in early stages and then shifted toward neutral emphasis (α = 0.55) in later generations. Similarly, we found β = 1% suitable initially and then steadily increased β to more than 6% in the final iterations, which permitted sufficient exploration of warping space while limiting errors. Although optimizing the algorithm for our data set required some trial and error, comparable results could be obtained with different parameter schedules and numbers of iterations. The only inputs specific to a particular map between a pair of optical logs were two prima facie tie points, one near the beginning and another near the end of the records, to seed the first pass through the warping engine.

[13] We had previously identified common features between the optical logs from Holes 21 and 50 through laborious visual inspection, which we compared against output from the DTW routine while fine tuning the algorithm. In many cases we found that the DTW correctly mapped features that had been misidentified during visual inspection. We also developed the algorithm using Monte Carlo generated test data, both with and without amplitude noise. A representative subsample of interhole maps obtained using the DTW routine is plotted in Figure 3.

[14] To determine chronology of the records (Figure 4) we mapped all dust data onto a common depth of the uphole log

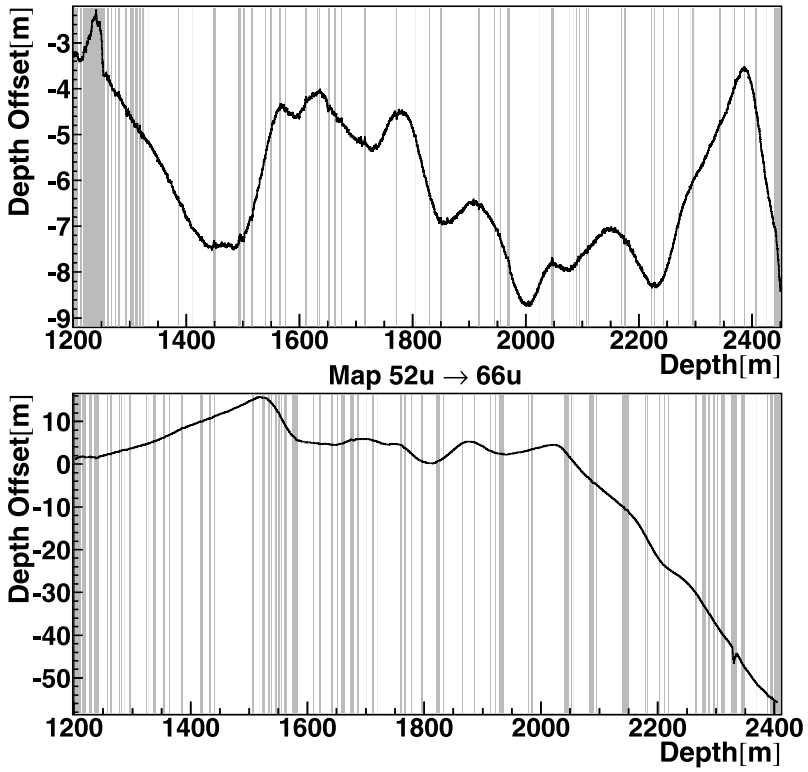

Figure 5. Example maps between optical logs, showing shaded error intervals excluded by automated internal consistency checks. (top) The error on the top left was caused by a cavern in Hole 2 created by the hot-water dill; (bottom) the error near 2330 m was a data gap in the Hole 52 log.

in Hole 10, then used a coarse DTW algorithm to synchronize with dust measured in the EDML and EDC ice cores [*Ruth et al.*, 2007]. Based on this age scale we predict that ice from the Eemian period, the last interglacial ca. 130 to 114 ka, should be accessible at South Pole. We note little curvature in the age versus depth curve and make no corrections for thinning.

3.2. Error Suppression

[15] The dynamic mapping method can be somewhat unstable and susceptible to being thrown off-track, leading to intervals of false association. The problem was exacerbated by errors in the optical profiles themselves, such as data gaps or signal distortion in borehole caverns formed when the hot-water drill dwelled at one depth. The resulting errors were typically much larger than any surface roughness signal; if not objectively identified and removed these errors would propagate through the analysis and corrupt the measurement. Data gaps, mechanical oscillations of the logging tool detected in the pressure signal, and logging intervals otherwise known to be faulty were identified and removed as part of initial data cleaning. To discriminate and excise remaining errors, we employed a system of internal consistency checks.

[16] Surface features are best characterized through a composite over many different surface locations, since a comparison at just two points is unlikely to capture the average roughness magnitude. We built the final signal from the 41 maps between different boreholes, out of $\frac{10\times9}{2} = 45$ possible pairwise combinations of 10 optical profiles in 6 holes. To isolate errors we cross-checked maps in triplets for internal consistency, as in equation (11) of *Barnes et al.* [2006]:

$$\delta_{ij} - \delta_{ik} + \delta_{jk} = (z_i - z_j) - (z_i - z_k) + (z_j - z_k) = 0 \qquad (3)$$

If multiple maps concur on which features should be matched the residuals vanish. Any particular map between two dust records can be reconciled with maps to a third record drawn from the other eight. We calculated equation (3) at each point of $\frac{45\times8}{3} = 120$ error reports, then stacked reports for the 41 maps in order to isolate discrepant intervals that consistently produced significant residuals or a paucity of zero-crossings in comparisons. We flagged for excision any interval of any map deemed suspect in >75% of triplet consistency checks, which removed ~18% of the total data set from the resultant signal. Example maps and excised error templates are plotted in Figure 5. We compared two parallel analysis chains, with the second more stringent set of cuts removing an average of 12% and as much as 25% larger portions of the maps from the analysis, to evaluate whether the data had been sufficiently cleaned and also test for artifacts introduced by the error suppression. We examine potential systematics in section 3.4.

3.3. Surface Roughness Signal Compilation

[17] We compiled our surface roughness record as the standard deviation of isochrone depth obtained from all pairwise mappings surviving error suppression in a given time bin. Isochrone offsets of meters to tens of meters, which

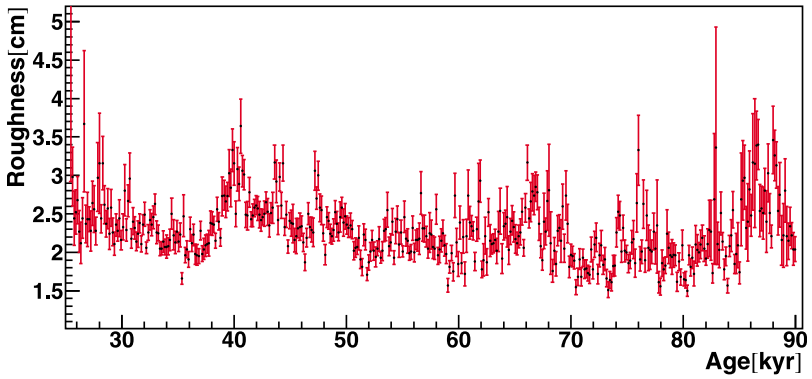

Figure 6. South Pole composite surface roughness record in 150 year bins, with bootstrapped statistical error bars.

develop over tens to hundreds of meters in depth, resulted from bulk glacial flow or perhaps larger landforms such as megadunes. Smaller aeolian roughness features, sculpted to a few decimeters tall at the surface and subsequently compressed during firn densification, are barely perceptible at the scales of Figures 3 and 5. After masking portions of the maps from consideration with the error templates, we subtracted a spline fit from each map to remove larger flow distortions and harvest small features, which we placed on a common age scale with 50 or 150 year binning. We applied a factor $\sqrt{\frac{\pi}{2}}$ to convert positive gaussian mean deviation to standard deviation of isochrone depth or RMS roughness (comparable to *Barnes et al.* [2006] σ_{Δ}). We used a bootstrap method [*Chernick*, 2008] to compile roughness measurements and derive the statistical error bars shown in Figure 6. We formed the composite on a borehole basis, weighting two logs from the same hole by $\frac{1}{2}$ each and the single logs from Holes 21 and 50 by unity.

3.4. Systematics

[18] Intervals of high dust, when the surface was presumably more distorted by higher winds, were less easy to synchronize than periods of low to moderate dust, in both the automated and manual analyses. Fewer measurements tended to survive internal consistency checking, and matching features by eye became more challenging, when dust levels were highest. The sizes of the error bars in Figure 6 reflect this potential systematic effect.

[19] In Figure 7 we compare our roughness with the record by *Barnes et al.* [2006] at Dome C, in the overlapping interval 44 to 26 ka. The resemblance between records is striking, with nearly the same average level of roughness derived from two different measurements and analyses. Although certain variations of the two signals may correspond, the measurement by *Barnes et al.* [2006] was based on a single comparison between two core electrical conductivity records and understandably contains more noise. Nonetheless the apparent uniformity in surface roughness across the East Antarctic Plateau is remarkable, which we address further in the next section.

[20] In order to evaluate whether sufficient data had been collected and to test stability against measurement and analysis artifacts, we examined consistency of the signal derived from distinct subsets of data. In the top panel of Figure 8, we divided the data set approximately in half, assigning the Hole 50 and all uphole logs to one set, and the Hole 21 and remaining downhole logs to the other set. This resulted in $\frac{5\times4}{2} = 10$ maps each instead of the 41 in the full sample. The subrecords contained more statistical noise, and were not strictly independent since we used the same error templates that we derived for the full sample. In the bottom panel we compare the roughness records we obtained before and after internal consistency cleaning.

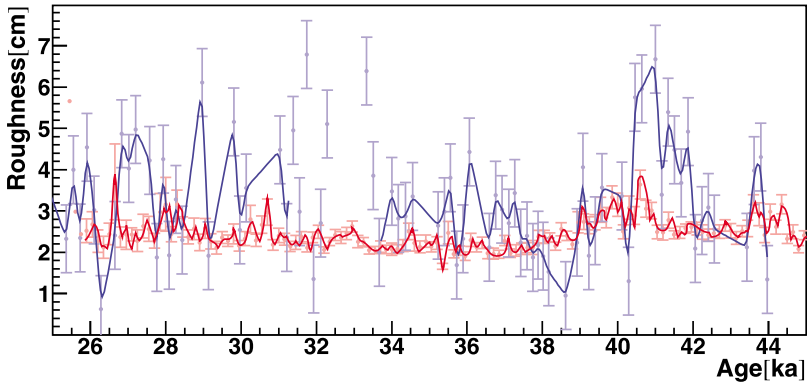

Figure 7. Comparison of our paleoroughness record (red) with that of *Barnes et al.* [2006] at Dome C (blue). The solid curves are 150-year Gaussian averages.

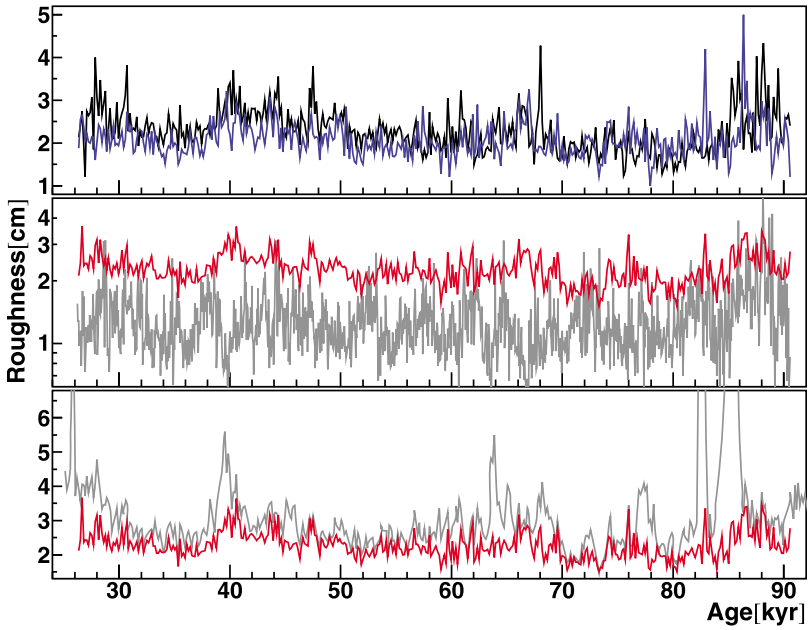

Figure 8. (top) Roughness signals in 50 year bins constructed from only upgoing logs together with Hole 50 (blue), overlayed with the signal using only downgoing logs and Hole 21 (black). Each comprises $\frac{5\times4}{2} = 10$ maps compared with 41 in the full sample, while the error suppression templates used were those derived from the entire data set. (middle) Full composite roughness record (red) and that resulting only through comparisons of upgoing and downgoing optical logs from the same borehole (gray) on a logarithmic scale. (bottom) Wind record with error suppression (red) and without (gray).

[21] The laser illuminates 60° of the horizon at a time. Due to free rotations of the cable the beam can shine into different ice in separate passes of the probe. Particularly in bubble-free ice with relatively low dust content, where the seeing distance is greatest, an attenuated roughness signal could be detectable in two logs of the same hole. In the middle panel of Figure 8 we compare our full composite measurement to the roughness derived from the four comparisons between up- and downgoing optical logs in Holes 2, 10, 52 and 66. Some of the roughness signal appears to have been reproduced in the single-borehole analysis, though at smaller amplitude.

4. Discussion

[22] *Bagnold* [1941] and later *Wilson* [1972] concluded that sand dunes are not merely larger versions of sand ripples, since the lack of any intermediate-size features implies that the two have different formation mechanisms: ripples are produced by saltating grains and dunes from more complicated aerodynamics. Since a snow surface is a cohesive yet breakable matrix of bonded crystals, snow saltation differs from that of sand and soil [*Pomeroy and Gray*, 1990]. We have suppressed features larger than ~20 cm, which would have been of order a half-meter tall or more when on the surface. At high wind speeds, saltating snow could become abrasive and obliterate smaller surface features so that the wind-sastrugi relationship breaks down. *McConnell et al.* [1997] monitored South Pole accumulation monthly for a period of seven years, over a 50 by 60 m array of stakes. They found a spatial accumulation standard deviation in the range 1 to 7 cm that appeared to track monthly peak wind speed. *Gow* [1964] noted that South Pole surface relief which formed during winter did not seem to persist through the entire year, but appeared worn down by summer sublimation and deflation. *Palais et al.* [1982] observed accumulation at Dome C occurring mostly in winter, while summer could be characterized mainly as a season of ablation.

[23] *Fischer et al.* [2007a] concluded that dust in Dome C ice only slightly overrepresented atmospheric concentration. Since the flux and residence time of air through snow are functions of wind speed and surface roughness, these might impact dry deposition directly through a filtration effect [*Harder et al.*, 1996]. The modern South Pole accumulation rate is atypically high for the Antarctic Plateau and may include a significant wet deposition component. We overlay surface roughness with the South Pole dust signal in Figure 9, with dust averaged over all measurements and plotted on a logarithmic scale. Based on this facile comparison, circulation intensity by itself would not appear to explain the largest dust increases, though of course we cannot rule out upper level transport effects. We have not made any corrections to our record for ice provenance, thinning or changes in accumulation rate. By accounting for the break in the age versus depth curve near 60 ka, for example, the wind-dust correlation in the ca. 63 ka dust peak might be improved. While the correlation between surface roughness and dust was significant, the signals did not track perfectly and at times even appear to have been out of phase. Such a halting relationship would be consistent with findings that increases in dust supply at the source regions were largely responsible for the variations in Antarctic deposition [*Sugden et al.*, 2009; *Fischer et al.*, 2007b].

[24] Quantitative conversion of roughness to surface wind speed will require further study. *Barnes et al.* [2006] noted

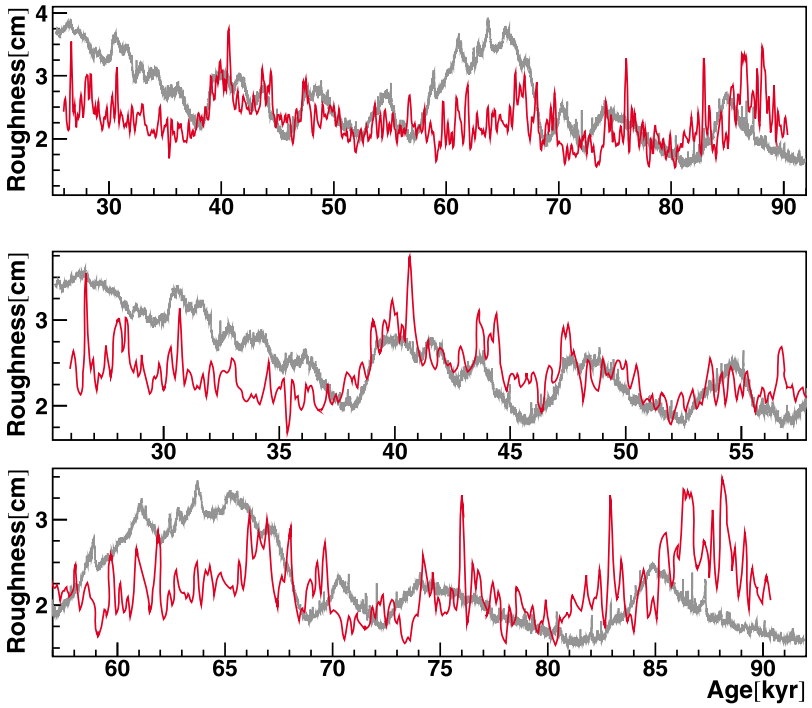

Figure 9. South Pole surface roughness record, in 50 year bins with 200-year Gaussian averaging (red), overlayed with the logarithm of the average dust signal (gray), over three time intervals: (top) the entire record, (middle) 58 to 26 ka, and (bottom) 90 to 57 ka.

that accumulation rate, temperature and wind speed may be correlated, and furthermore that accumulation rate and temperature may influence sastrugi height. *Barnes et al.* [2006] remarked on the surprising lack of variation in their surface roughness profile over different climates. We also measured a dynamic range of only a factor ~few over the entire record. Typically accumulation would have been suppressed during cold phases, possibly limiting sastrugi growth and diminishing the wind signal. The agreement between our record and that of *Barnes et al.* [2006] in the overlapping interval between 26 ka and 44 ka is noteworthy (Figure 7). The roughness preserved at the two sites was of comparable magnitude, even though Dome C is 1700 km away with an accumulation rate one quarter that of South Pole. South Pole lies downslope from the East Antarctic Plateau and generally experiences stronger, more steady katabatic winds than are typical within the polar high. At sites such as Dome C without a dominant prevailing wind, sastrugi can be absent (J. Schwander, personal communication, 2008) since nascent landforms tend not to grow if the wind direction is continually changing. The typical katabatic wind at South Pole is grid northeast, the result of coriolis redirection of air flowing from the eastern high. However, judging from decades of year-round meteorological observations, it is storm activity, typically off the Weddell Sea to the northwest, that is responsible for high wind events and most accumulation at South Pole (T. Markle, personal communication, 2009). The frequency and intensity of storms impinging on the coasts may be the dominant factor controlling both accumulation and surface roughness in the interior of Antarctica over long time periods.

[25] To compare our roughness record with other environmental variables, we invert the signal as a smoothness parameter (roughness^{-1}). In Figure 10 we plot the South Pole wind intensity signal alongside Antarctic $\delta^{18}O$ and CO_2 [*Blunier and Brook*, 2001; *Ahn and Brook*, 2008]. Typically near-surface local wind speed and temperature are positively correlated at Antarctic sites, so the anti-correlation with temperature we have found indicates a different mechanism. Modeling studies have pointed to a relationship between climate and the position of the westerlies, in which warmer climates have poleward shifted westerlies while cold climates like the LGM had westerlies shifted toward the equator. *Toggweiler et al.* [2006] suggested that reorganizations of ocean circulation during the last glacial were connected to changes in wind forcing around Antarctica. *Williams and Bryan* [2006] found that an equatorward shift of the westerlies during cold periods should be accompanied by stronger easterlies, including the polar easterlies, to conserve angular momentum. We include at the bottom of Figure 10 the recently published Southern Ocean upwelling proxy of *Anderson et al.* [2009], where they argued that reorganization of atmospheric circulation led to enhanced ocean upwelling around Antarctica and was the key driver of increased glacial CO_2 levels. *Anderson et al.* [2009] used biogenic opal from sediment cores as proxy for nutrient supply by ocean upwelling, which they claimed tracked shifts in the wind system of the Southern Hemisphere, particularly migration of the SH westerlies and wind stress levels at the latitude of the Drake Passage.

[26] We propose that interior Antarctic surface roughness was a reflection of wider climate, with higher peak winds associated with secular northward migrations of the westerlies and decreasing atmospheric CO_2. By contrast, during southward migrations of the westerlies, characterized by a

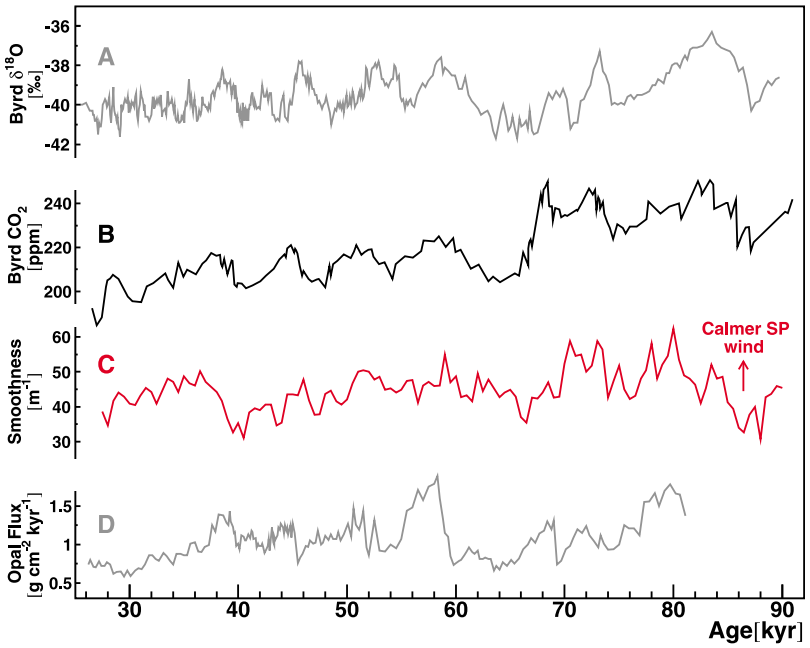

Figure 10. (c) Inverted South Pole wind intensity (smoothness ≡ roughness^{-1}, in 500-year bins, red), compared to Byrd (a) $\delta^{18}O$ and (b) CO_2 [*Blunier and Brook*, 2001; *Ahn and Brook*, 2008], and (d) the opal Southern Ocean upwelling proxy of *Anderson et al.* [2009].

more vigorous Antarctic Circumpolar Current and enhanced Southern Ocean upwelling, the Antarctic interior was isolated with calmer winds. *Udisti et al.* [2004] measured a changing ratio of Dome C-Vostok accumulation over the last glacial, with a prominent inflection in the ratio around ~38 ka. *Udisti et al.* [2004] postulated that atmospheric reorganization was responsible for a more intense and persistent polar vortex during cold phases, which presented a barrier against mid-latitude air masses penetrating Antarctica. *Barnes et al.* [2006] measured a pronounced decrease in roughness around 17 ka, which postdates our measurement yet similarly coincided with an upwelling pulse of *Anderson et al.* [2009]. These results fill a gap by providing direct measurements of paleowind intensity at Earth's South Pole and the Antarctic Plateau, as possible evidence that the SH wind system governed glacial period deep water ventilation and pCO_2. This new parameter could help disentangle the biochemical and physical controls of climate, with implications for future uptake of atmospheric CO_2 by the ocean.

[27] The use of South Pole ice for the construction of a major particle physics detector permitted this analysis of several deep glacial boreholes in close proximity. The ice coring community is investigating the development of replicate coring technology, in which the drill would be diverted from the main borehole in order to retrieve ice samples from short intervals deemed to be of particular interest. The rare circumstances of the present study raise the prospects for a multi-*core* approach to deep ice research, exemplifying the potential economy of scale and scientific gain from retrieving multiple unabridged deep cores at each drilling site.

[28] **Acknowledgments.** We thank Tim Markle, Ed Brook, Jakob Schwander, Jinho Ahn, Kirill Filimonov, Eric Wolff, and Bob Hawley for insightful discussion. Three anonymous reviewers improved the paper. We are grateful to the members of the IceCube collaboration for their support and splendid performance, in particular Tom Ham, Mark Thoma, Andres Morey, and the Enhanced Hot Water Drill team. This research was supported by the U. S. National Science Foundation (Office of Polar Programs and Physics Division), University of Wisconsin Alumni Research Foundation, U.S. Department of Energy, National Energy Research Scientific Computing Center, Louisiana Optical Network Initiative (LONI) grid computing resources; National Science and Engineering Research Council, Canada; Swedish Research Council, Swedish Polar Research Secretariat, Swedish National Infrastracture for Computing (SNIC), Knut and Alice Wallenberg Foundation, Sweden; German Ministry for Education and Research (BMBF), Deutsche Forschungsgemeinschaft (DFG), Research Department of Plasmas with Complex Interactions (Bochum), Germany; Fund for Scientific Research (FNRS-FWO), FWO Odysseus programme, Flanders Institute to Encourage Scientific and Technological Research in Industry (IWT), Belgian Federal Science Policy Office (Belspo); Marsden Fund, New Zealand; Japan Society for Promotion of Science (JSPS); the Swiss National Science Foundation (SNSF), Switzerland; EU Marie Curie OIF Program; and Capes Foundation, Ministry of Education, Brazil.

References

Ackermann, M., et al. (2006), Optical properties of deep glacial ice at the South Pole, *J. Geophys. Res.*, *111*, D13203, doi:10.1029/2005JD006687.

Ahn, J., and E. J. Brook (2008), Atmospheric CO_2 and climate on millennial time scales during the last glacial period, *Science*, *322*, 83–85.

Anderson, R. F., S. Ali, L. I. Bradtmiller, S. H. H. Nielsen, M. Q. Fleisher, B. E. Anderson, and L. H. Burckle (2009), Wind-driven upwelling in the Southern Ocean and the deglacial rise in atmospheric CO_2, *Science*, *323*, 1443–1447.

Bagnold, R. A. (1941), *The Physics of Blown Sand and Desert Dunes*, Methuen, London.

Barnes, P. R. F., E. W. Wolff, and R. Mulvaney (2006), A 44 kyr paleoroughness record of the Antarctic surface, *J. Geophys. Res.*, *111*, D03102, doi:10.1029/2005JD006349.

Bay, R. C., N. E. Bramall, P. B. Price, G. D. Clow, R. L. Hawley, R. Udisti, and E. Castellano (2006), Globally synchronous ice core volcanic tracers and abrupt cooling during the last glacial period, *J. Geophys. Res.*, *111*, D11108, doi:10.1029/2005JD006306.

Bingham, R. G., M. J. Siegert, D. A. Young, and D. D. Blankenship (2007), Organized flow from the South Pole to the Filchner-Ronne ice shelf: An assessment of balance velocities in interior East Antarctica using radio echo sounding data, *J. Geophys. Res.*, *112*, F03S26, doi:10.1029/2006JF000556.

Blunier, T., and E. J. Brook (2001), Timing of millennial-scale climate change in Antarctica and Greenland during the last glacial period, *Science*, *291*, 109–112.

Bramall, N. E., R. C. Bay, K. Woschnagg, R. A. Rohde, and P. B. Price (2005), A deep high-resolution optical log of dust, ash, and stratigraphy in South Pole glacial ice, *Geophys. Res. Lett.*, *32*, L21815, doi:10.1029/2005GL024236.

Brook, E. J., J. W. C. White, A. S. M. Schilla, M. L. Bender, B. Barnett, J. P. Severinghaus, K. C. Taylor, R. B. Alley, and E. J. Steig (2005), Timing of millennial-scale climate change at Siple Dome, West Antarctica, during the last glacial period, *Quat. Sci. Rev.*, *24*, 1333–1343.

Chernick, M. R. (2008), *Bootstrap Methods: A Guide for Practitioners and Researchers*, 369 pp., John Wiley, Hoboken, N. J.

EPICA community members (2004), Eight glacial cycles from an Antarctic ice core, *Nature*, *429*, 623–628.

EPICA community members (2006), One-to-one coupling of glacial climate variability in Greenland and Antarctica, *Nature*, *444*, 195–198.

Fischer, H., M.-L. Siggaard-Andersen, U. Ruth, R. Röthlisberger, and E. Wolff (2007a), Glacial/interglacial changes in mineral dust and sea-salt records in polar ice cores: Sources, transport, and deposition, *Rev. Geophys.*, *45*, RG1002, doi:10.1029/2005RG000192.

Fischer, H., et al. (2007b), Reconstruction of millennial changes in dust emission, transport and regional sea ice coverage using the deep EPICA ice cores from the Atlantic and Indian Ocean sector of Antarctica, *Earth Planet. Sci. Lett.*, *260*, 340–354.

Giovinetto, M. B., D. H. Bromwich, and G. Wendler (1992), Atmospheric net transport of water vapor and latent heat across 70°S, *J. Geophys. Res.*, *97*(D1), 917–930, doi:10.1029/91JD02485.

Gow, A. J. (1964), On the accumulation and seasonal stratification of snow at the South Pole, *J. Glaciol.*, *5*(40), 467–477.

Harder, S. L., S. G. Warren, R. J. Charlson, and D. S. Covert (1996), Filtering of air through snow as a mechanism for aerosol deposition to the Antarctic ice sheet, *J. Geophys. Res.*, *101*(D13), 18,729–18,743.

Hogan, A. W., and A. J. Gow (1997), Occurrence frequency of thickness of annual snow accumulation layers at South Pole, *J. Geophys. Res.*, *102*(D12), 14,021–14,027.

Kawamura, K., J. P. Severinghaus, S. Ishidoya, S. Sugawara, G. Hashida, H. Motoyama, Y. Fujii, S. Aoki, and T. Nakazawa (2006), Convective mixing of air in firn at four polar sites, *Earth Planet. Sci. Lett.*, *244*, 672–682.

Keogh, E., and M. J. Pazzani (2000), Scaling up dynamic time warping for datamining applications, paper presented at Sixth ACM SIGKDD International Conference on Knowledge Discovery and Data Mining, Assoc. for Comput. Mach., Boston, Mass.

Kogan, J. A., and D. Margoliash (1998), Automated recognition of bird song elements from continuous recordings using dynamic time warping and hidden Markov models: A comparative study, *J. Acoust. Soc. Am.*, *103*(4), 2185–2196.

Mahesh, A., R. Eager, J. R. Campbell, and J. D. Sphinhirne (2003), Observations of blowing snow at the South Pole, *J. Geophys. Res.*, *108*(D22), 4707, doi:10.1029/2002JD003327.

Marino, F., et al. (2008), Defining the geochemical composition of the EPICA Dome C ice core dust during the last glacial-interglacial cycle, *Geochem. Geophys. Geosyst.*, *9*, Q10018, doi:10.1029/2008GC002023.

McConnell, J. R., R. C. Bales, and D. R. Davis (1997), Recent intra-annual snow accumulation at South Pole: Implications for ice core interpretation, *J. Geophys. Res.*, *102*(D18), 21,947–21,954.

Palais, J. M., I. M. Whillans, and C. Bull (1982), Snow stratigraphic studies at Dome C, East Antarctica: An investigation of depositional and diagenetic processes, *Ann. Glaciol.*, *3*, 239–242.

Petit, R., et al. (1999), Climate and atmospheric history of the past 420,000 years from the Vostok ice core, Antarctica, *Nature*, *399*, 429–436.

Pomeroy, J. W., and D. M. Gray (1990), Saltation of snow, *Water Resour. Res.*, *26*(7), 1583–1594.

Roberts, K., P. Lawrence, A. Eisen, and M. Hoirch (1987), Enhancement and dynamic time warping of somatosensory evoked potential components applied to patients with multiple sclerosis, *IEEE Trans. Biomed. Eng.*, *34*(6), 397–405.

Ruth, U., et al. (2007), EDML1: A chronology for the EPICA deep ice core from Dronning Maud Land, Antarctica, over the last 150000 years, *Clim. Past*, *3*, 475–484.

Sakoe, H., and S. Chiba (1978), Dynamic programming algorithm optimization for spoken word recognition, *IEEE Trans. Acoust. Speech Signal Process.*, *26*(1), 43–49.

Salvador, S., and P. Chan (2004), FastDTW: Toward accurate dynamic time warping in linear time and space, paper presented at Workshop on Mining Temporal and Sequential Data, Assoc. for Comput. Mach., Seattle, Wash.

Sugden, D. E., R. D. McCulloch, A. J. -M. Bory, and A. S. Hein (2009), Influence of Patagonian glaciers on Antarctic dust deposition during the last glacial period, *Nat. Geosci.*, *2*, 281–85.

Toggweiler, J. R., J. L. Russell, and S. R. Carson (2006), Midlatitude westerlies, atmospheric CO_2, and climate change during the ice ages, *Paleoceanography*, *21*, PA2005, doi:10.1029/2005PA001154.

Udisti, R., S. Becagli, E. Castellano, B. Delmonte, J. Jouzel, J. R. Petit, J. Schwander, B. Stenni, and E. W. Wolff (2004), Stratigraphic correlations between the European Project for Ice Coring in Antarctica (EPICA) Dome C and Vostok ice cores showing the relative variations of snow accumulation over the past 45 kyr, *J. Geophys. Res.*, *109*, D08101, doi:10.1029/2003JD004180.

van den Broeke, M. (2008), Depth and density of the Antarctic firn layer, *Arct. Antarct. Alp. Res.*, *40*(2), 432–438.

van der Veen, C. J., E. Mosley-Thompson, A. J. Gow, and B. G. Mark (1999), Accumulation at South Pole: Comparison of two 900-year records, *J. Geophys. Res.*, *104*(D24), 31,067–31,076.

Wang, K., and T. Gasser (1997), Alignment of curves by dynamic time warping, *Ann. Stat.*, *25*(3), 1251–1276.

Williams, G. P., and K. Bryan (2006), Ice age winds: An aquaplanet model, *J. Clim.*, *19*, 1706–1715.

Wilson, I. G. (1972), Universal discontinuities in bedforms produced by the wind, *J. Sediment. Petrol.*, *42*(3), 667–669.

Winkler, I., G. P. Háden, O. Ladinig, I. Sziller, and H. Honing (2008), Newborn infants detect the beat in music, *Proc. Nat. Acad. Sci. U. S. A.*, *106*, 2468–2471.

Witkin, A., D. Terzopoulos, and M. Kass (1987), Signal matching through scale space, *Int. J. Comput. Vision*, *1*(2), 133–144.

R. C. Bay, P. B. Price, and R. A. Rohde, Department of Physics, University of California, Berkeley, 366 LeConte Hall, Berkeley, CA 94720, USA. (bay@berkeley.edu)

N. E. Bramall, NASA Ames Research Center, Moffett Field, CA 94035, USA.